Highly strained AlAs-type interfaces in InAs/AlSb heterostructures

Maxime Vallet, Yann Claveau, Bénédicte Warot-Fonrose, Christophe Gatel, Julien Nicolaï, Nicolas Combe, C. Magen, R. Teissier, A. N. Baranov, Anne Ponchet

Highly strained AlAs-type interfaces in InAs/AlSb heterostructures

M. Vallet, Y. Claveau, B. Warot-Fonrose, C. Gatel, J. Nicolai, N. Combe, C. Magen, R. Teissier, A. N. Baranov, and A. Ponchet

Citation: Appl. Phys. Lett. **108**, 211908 (2016); doi: 10.1063/1.4952951

View online: https://doi.org/10.1063/1.4952951

View Table of Contents: http://aip.scitation.org/toc/apl/108/21

Published by the American Institute of Physics

Highly strained AlAs-type interfaces in InAs/AlSb heterostructures

M. Vallet,[1,2,a)] Y. Claveau,[1] B. Warot-Fonrose,[1,2] C. Gatel,[1,2] J. Nicolai,[1,2] N. Combe,[1] C. Magen,[2,3] R. Teissier,[4] A. N. Baranov,[4] and A. Ponchet[1,2]
[1]*CEMES CNRS-UPR 8011, Université de Toulouse, 29 rue Jeanne Marvig, 31055 Toulouse, France*
[2]*Transpyrenean Associated Laboratory for Electron Microscopy (TALEM), CEMES-INA, CNRS-Universidad de Zaragoza, Toulouse, France*
[3]*Laboratorio de Microscopias Avanzadas (LMA), Instituto de Nanociencia de Aragon (INA)—ARAID and Departamento de Fisica de la Materia Condensada, Universidad de Zaragoza, 50018 Zaragoza, Spain*
[4]*Institute of Electronics and Systems, UMR 5214 CNRS – University of Montpellier, 34095 Montpellier, France*

(Received 14 April 2016; accepted 17 May 2016; published online 26 May 2016)

Spontaneously formed Al-As type interfaces of the InAs/AlSb system grown by molecular beam epitaxy for quantum cascade lasers were investigated by atomic resolution scanning transmission electron microscopy. Experimental strain profiles were compared to those coming from a model structure. High negative out-of-plane strains with the same order of magnitude as perfect Al-As interfaces were observed. The effects of the geometrical phase analysis used for strain determination were evidenced and discussed in the case of abrupt and huge variations of both atomic composition and bond length as observed in these interfaces. Intensity profiles performed on the same images confirmed that changes of chemical composition are the source of high strain fields at interfaces. The results show that spontaneously assembled interfaces are not perfect but extend over 2 or 3 monolayers. *Published by AIP Publishing*. [http://dx.doi.org/10.1063/1.4952951]

Interfacial strained layers are present in some systems epitaxially grown as InAs/GaSb,[1] InAs/AlSb,[2,3] or ZnTe/CdSe,[4,5] due to the lack of common atomic species between the two materials. They may affect the electronical and optical properties especially when the active zones are of nanometric size.[6,7] In the InAs/AlSb system that is widely used for short wavelength quantum cascade lasers (QCLs),[8] these interfacial layers may result in huge and very-localized strain variations due to the formation of Al-As or In-Sb bonds. While the lattice mismatch between InAs and AlSb is moderate (1.3%), it is −6.6% or +6.9% between InAs (the substrate) and AlAs or InSb (as bulk materials), respectively.[9] Depending on the dominant bond type, Al-As or In-Sb, the stress states at interfaces are then tensile or compressive, respectively. The strain can thus be used as a probe to explore the chemical nature of interfaces. In a previous study, interfaces in InAs/AlSb multilayers grown by molecular beam epitaxy (MBE) were qualitatively studied by combining strain profiles with chemical analysis performed on images captured by high resolution transmission electron microscopy (HRTEM) and high-angle annular dark field scanning transmission electron microscopy (HAADF-STEM), respectively.[2,3] The preferential formation of tensile AlAs-type interface due to its higher thermal stability in comparison with InSb-type was observed.

The aim of this article is to determine the extension of these interfaces, and how their Al-As character is marked. In QCLs, the thicknesses of both AlSb and InAs layers tune directly the light emission through the electronic structure. They are frequently in the range of 1–2 nm,[8] so that the role of interfaces becomes significant. For this purpose, we studied a sample grown using a simple procedure chosen to favor the spontaneous formation of interfaces, and we focused on the meaning of the measured strain at these interfaces. The geometrical phase analysis (GPA) of atomically resolved images, which relies on a filtering in the Fourier space of the image, has become a standard method well adapted for strain analysis of nanometric layers with a moderate strain gradient.[10] However, its application to interfaces with abrupt and huge variations of both atomic composition and bond length requires some caution. In particular, we intend to discuss the ability of determining the actual level of strain in that case. For this purpose, a strain analysis was performed on atomically resolved Z-contrast images acquired by HAADF-STEM and using an improved process of image acquisition, which removes the detrimental effects of image drifts and scan errors. Experimental strain profiles were then compared to those obtained from images generated from model structures, with a focus on the effect of convolution due to the mask used in the GPA treatment. The HAADF-STEM was also chosen to correlate strain and qualitative chemical information from the same image. The scattered intensity indeed varies with the atomic number of elements Z (intensity varies as Z^n, with n close to 1.7).[11,12] The combination of strain and intensity profiles allowed us to infer the width of interfaces and their high content in AlAs bonds.

The sample was grown on (001) InAs substrate by MBE at 700 K with a growth rate of 1 Å s^{-1} and a V/III flux ratio of about 2. Thicknesses of AlSb and InAs layers were set to 4 and 20 nm, respectively, in order to clearly separate strain fields induced by two successive interfaces while keeping a fully strained structure. A growth interruption of 3 s without V element flux was performed at interfaces. Cross-sectional TEM samples along the [110] and [1$\bar{1}$0] zone axes were prepared by mechanical polishing and argon ion milling at low temperature. HAADF-STEM was performed using a FEI Titan 60–300 operated at 300 kV and equipped with a high brightness field emission gun (X-FEG), a Wien filter monochromator, and a

a)Author to whom correspondence should be addressed. Electronic mail: maxime.vallet@cemes.fr

probe aberration corrector reaching a spatial resolution of 0.08 nm in STEM. To prevent scan distortions due to the drift of the sample and to minimize the effect of the scan error, series of 20 images of 1024 × 1024 pixels were acquired using a speed rate of 0.8 μs/pixel. They were then aligned using cross correlation methods and finally summed. High quality images with a good signal-to-noise ratio were then obtained.

The strain states were determined using the GPA method.[10] Circular masks with a cosine profile were used in the reciprocal space of images to select two non-collinear reciprocal lattice vectors **g** required to determine the 2D strain field. The $\mathbf{g} = 220$ and $\mathbf{g} = 004$ vectors were used to prevent additional phase shifts at interfaces that occur in HAADF-STEM images of materials with compositionally distinct atom columns.[13] In the theory of linear elasticity and for a fully strained layer, the in-plane and out-of-plane strain components $\varepsilon_{//}^{abs}$ and $\varepsilon_{\perp}^{abs}$ are expressed as a function of the lattice mismatch f as

$$\varepsilon_{//}^{abs} = -f \text{ and } \varepsilon_{\perp}^{abs} = 2\frac{C_{12}}{C_{11}}f \text{ where } f = \frac{a_l - a_s}{a_s}, \quad (1)$$

where C_{12} and C_{11} are elastic constants of the material constituting the studied layer, a_l and a_s are the lattice parameters of the layer and the substrate, respectively. The local strains measured by GPA are relative to a reference area taken within the InAs layers far from the thin AlSb layer and, thus, assumed to be strain-free. The out-of-plane measured strain component $\varepsilon_{\perp}^{GPA}$ that is expressed relatively to the InAs lattice parameter is expected to be

$$\varepsilon_{\perp}^{GPA} = \varepsilon_{\perp}^{abs} + f = f\left[1 + 2\frac{C_{12}}{C_{11}}\right]. \quad (2)$$

Figure 1(a) shows a [1$\bar{1}$0] zone axis image of the sample. The InAs and AlSb layers are clearly distinguished and separated by thin homogeneous interfacial layers, referred as I1 and I2. Insets display magnified images of the InAs and AlSb layers. In InAs, dumbbells are readily resolved with In columns at the top and As ones at the bottom. In AlSb, the Al columns present a much weaker intensity in the top position of the dumbbell compared to Sb columns, due to the large difference of atomic number between Al (Z = 13) and Sb (Z = 51). As the image intensity is relative to Z, insight on the chemical composition variation can be obtained at a very local scale. Figure 1(b) exhibits two intensity line profiles of adjacent atomic rows along the [001] direction taken in the middle of Figure 1(a). The peaks of the V columns are clearly identified in the whole profiles (peaks to the left of each dumbbell). The peaks of the III columns (to the right of each dumbbell) are well resolved except in the AlSb area, due to the large difference in Z of Al and Sb. Interfaces are identified by a significant change in the intensity of either the III or V peak. The drops of intensity of III and V columns indicate a larger amount of Al than In and a larger amount of As than Sb at interfaces. For these two particular rows, I1 and I2 interfaces extend over about 2.5 and 3 monolayers, respectively (i.e., 0.75 and 0.9 nm). Note, however, that this analysis is very local and that fluctuations occur from one row to another.

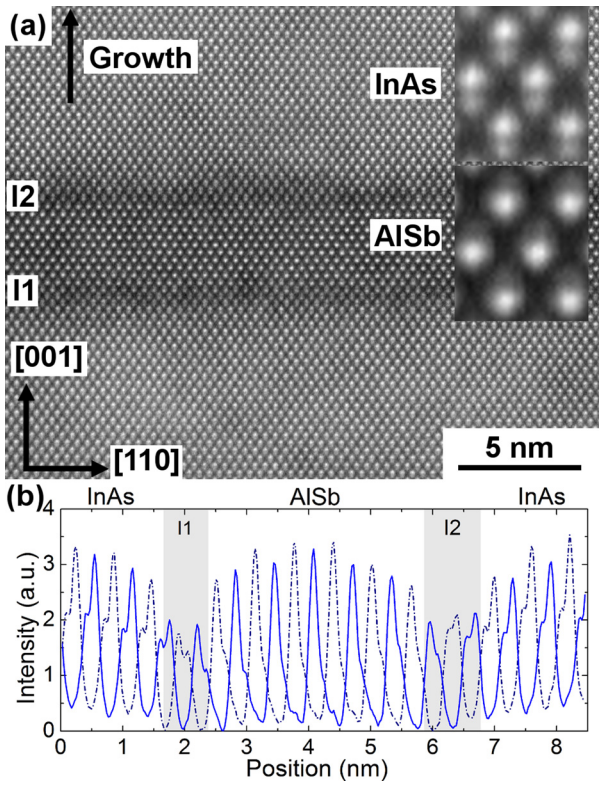

FIG. 1. (a) HAADF-STEM image along the [1$\bar{1}$0] zone axis of the InAs/AlSb system. I1 and I2 refer to the interfaces. Insets are higher magnifications of the InAs and AlSb layers. (b) Intensity line profiles along the growth direction taken in the middle of (a). Full and dotted lines come from two adjacent atomic rows.

In GPA analyses, the spatial resolution is partly limited by the size of the mask applied on the diffractogram resulting from the Fourier transform of the image. To examine this effect, five different mask sizes were used. The spatial resolution expressed in nanometer in the direct space of the images can be characterized by $R_S = 1/r$, where r is the mask radius in nm^{-1}. The in-plane measured strain in the [110] direction obtained from Figure 1(a) is homogeneous and null regardless the mask size (not shown here), confirming the perfect pseudomorphic growth of the layers. Figure 2 shows the out-of-plane strain ($\varepsilon_{\perp}^{GPA}$) maps and profiles of Figure 1(a) for three sizes of mask referred here as small (a), medium (b), and large (c), and indicated in yellow in the diffractograms. For these masks, R_S is 1 nm (a), 0.7 nm (b), and 0.45 nm (c), respectively. The large mask was chosen to have the largest possible radius in the reciprocal space without inducing artefacts due to the inclusion of more than one spot inside the mask (see inset of Figure 2(c)). Note that the best spatial resolution enabled by GPA in this structure corresponds to $R_S = 0.45$ nm; this value is smaller than the lattice parameter (around 0.6 nm) but larger than one monolayer (0.3 nm). It is important to note that an increase in the mask size for a better spatial resolution also corresponds to an increase of the noise and, thus, results in a lower signal-to-noise ratio. This effect is easily observed within the InAs areas assumed to be unstrained with $\varepsilon_{\perp}^{GPA}$ values at zero; the standard deviations are 0.25%, 0.32%, and 0.45% for masks (a), (b), and (c), respectively.

As can be seen in Figure 2, strain maps and profiles have the same appearance with the change of mask size.

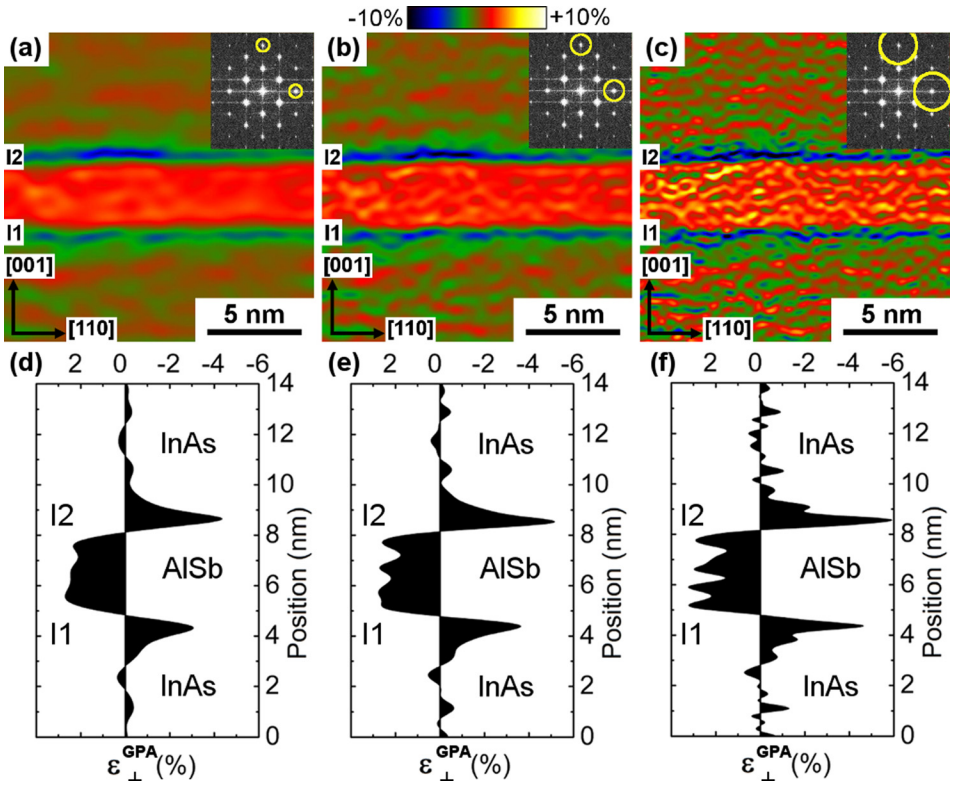

FIG. 2. Out-of-plane strain ($\varepsilon_{\perp}^{GPA}$) maps from the image of Figure 1(a) with spatial resolutions R_S of 1 nm (a), 0.7 nm (b), and 0.45 nm (c). The image diffractograms with the different mask sizes are shown in insets. Corresponding profiles of strain along the growth direction (integrated over the width of the image in the [110] direction) are displayed in (d), (e), and (f), respectively.

A compressive layer ($\varepsilon_{\perp}^{GPA} > 0$) surrounded by two tensile areas ($\varepsilon_{\perp}^{GPA} < 0$) is clearly observed in each case. The average value of the compressive layer, here 2.3%, does not change with the resolution. Average strains from 2.2% to 2.5% were measured on different images, in good agreement with the theoretical strain given by Eq. (2) (+2.5%) using elastic constants of AlSb, $C_{11} = 87.8$ GPa and $C_{12} = 43.5$ GPa.[9] However, at interfaces, the measured strain significantly changes with the improvement of the spatial resolution. At the I1 interface (AlSb on InAs), the measured strain evolves from −3.1% for the smallest mask (Figure 2(d)) to −4.6% for the largest one (Figure 2(f)). At the same time, the full-width at half-maximum (FWHM) of peaks is reduced from 0.77 nm to 0.44 nm. Similarly, at the I2 interface (InAs on AlSb), the measured strain increases from −4.3% (Figure 2(d)) to −5.9% (Figure 2(f)), while the FWHM is reduced from 0.72 nm to 0.47 nm. In other zones analyzed with the largest mask, the strain level reached −5% to −6%, and the fluctuations within one interface were comparable to the difference reported between I1 and I2 from Figure 1(a). The high negative strains measured for the largest mask in different images unambiguously point out a very high content in Al-As bonds at both interfaces. These values are much larger than the ones measured in previous studies performed by HRTEM on different samples grown under the same growth procedure as here (about −2% with the use of the medium mask).[2] Such differences can be attributed to the better signal-to-noise ratios of images achieved in this study compared to previous ones.

The strain profile was also compared to the intensity profile integrated over the width of the image in the [110] direction (Figure 3). The integrated intensity profile exhibits five different areas corresponding to the InAs layers (the brightest areas on both sides of the image), the AlSb layer, and interfacial layers. Interfacial layers are darker than InAs and AlSb, suggesting that both interfaces are AlAs-type interfaces in good agreement with the intensity line profiles (Figure 1(b)). Moreover, the minima of intensity at both interfaces correspond to the negative peaks of strain, confirming the fact that the highly tensile stressed areas coincide with the changes of chemical composition.

The effects of the mask size on the measured strain values at interfaces were then investigated on images generated from a model structure. Due to the strong AlAs-character of interfaces suggested by experimental results, a model of [InAs/AlSb] multilayer was built with perfect interfaces formed by one unique plane of Al-As bonds as schematized in Figure 4(a). The lattice parameter in the (001) plane was set to one of the unstrained InAs for the whole structure, while the lattice parameter in the [001] direction was calculated using the linear elasticity. For interfaces, elastic constants of bulk AlAs were used ($C_{11} = 125.5$ GPa and $C_{12} = 53.5$ GPa[9]). The expected out-of-plane strain profile was calculated from

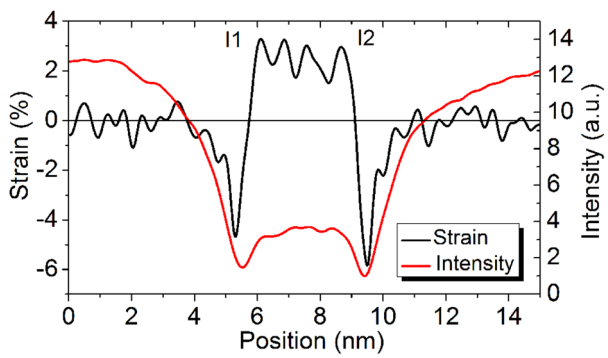

FIG. 3. Strain $\varepsilon_{\perp}^{GPA}$ and intensity profiles (respectively, in black and red) along the growth direction obtained from Figure 1(a). For both profiles, the image was filtered in the reciprocal space with the same mask size corresponding to a spatial resolution of R_S of 0.45 nm.

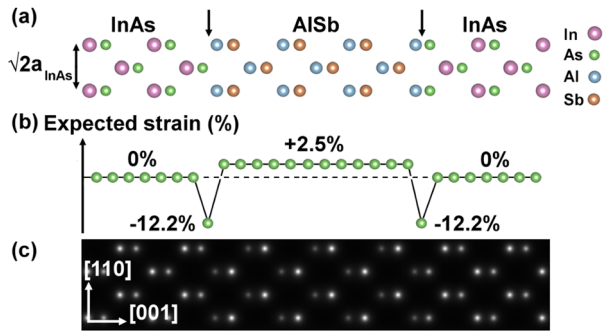

FIG. 4. Scheme of the InAs/AlSb system with pure AlAs interfaces in projection along [110] axis (a). Expected strain profile of this model structure using the InAs lattice parameter as reference (b). In (c), the model image of the structure from projected potentials.

Eq. (2) using the InAs lattice parameter as a reference (Figure 4(b)). A positive strain of +2.5% is expected in the AlSb layer, whereas high negative strain values (−12.2%) are expected at pure AlAs interfaces. An image of the structure shown in Figure 4(a) was generated using the projected potentials in the java electron microscopy software[14] (Figure 4(c)). This approach was chosen to get the exact position of atomic columns defined in the model. Differences between the measured strain and the expected strain profile will thus only come from the GPA method.

Strain maps and profiles of the model image analyzed with the same masks and **g** vectors as used for experiments are shown in Figure 5. As expected in the model, symmetric strain profiles composed of a positive plateau of +2.5% surrounded by two interfaces in tension are observed for different masks. At interfaces, the measured strain varies from −1.6% for the smallest mask (Figure 5(d)) to −6.3% for largest one (Figure 5(f)), while the FWHM of peaks is reduced from 0.54 nm to 0.23 nm. The exact strain value at these interfaces (−12.2%) can therefore not be measured even with the largest mask, i.e., with the best resolution allowed in GPA. Figure 6 shows the maxima of interfacial strain profiles from the experimental image of Figure 1(a) and the model one as a function of R_S, for the five mask sizes. All series of data show an increase of the measured strain at interfaces with the enlargement of the mask radius (improvement of R_S) demonstrating a similar effect of the mask. Close values of measured strain are obtained with the large masks. However, the model does not fully fit with the experimental interfaces. For small masks, the measured strain from experimental images (shown here or from other STEM images) is higher than those from the model image. In the same time, the FWHMs of interfacial peaks are systematically wider from the experimental image than from the simulated one (the difference being about 0.25 nm). The measured strain integrated over each interface is thus higher than that generated by the model of a pure Al-As interface. Considering the convolution effect induced by the mask, it can be inferred that the actual strain in the sample extends over more than one atomic plane and is close to the strain of pure AlAs as in the model without reaching it. Interfaces are thus constituted of an alloy with a very high content in AlAs. Strain maps and profiles were also performed from model images built with larger interfaces than in Figure 4. However, this does still not allow us to fully reproduce the decrease of measured strain with the mask size in experimental images. A limitation of this approach is due to the fact that TEM/STEM images are projections, and the same strain profiles could result either from imperfect interfaces with the formation of alloys or else from an interfacial roughness with perfect interfaces.

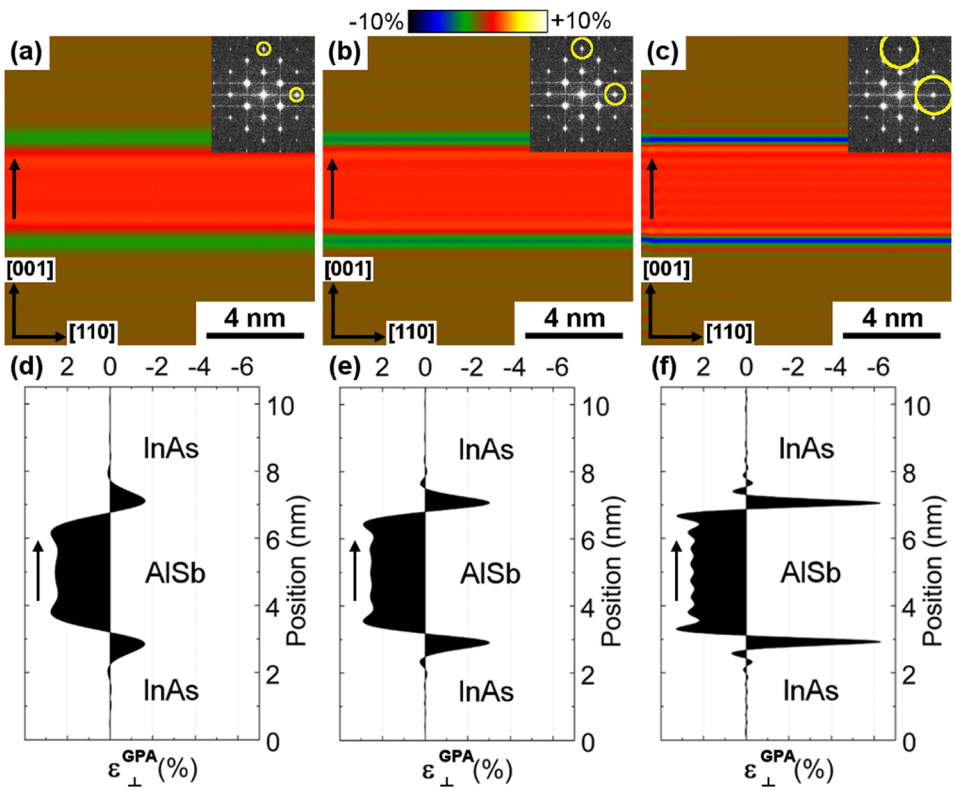

FIG. 5. Out-of-plane strain ($\varepsilon_{\perp}^{GPA}$) maps from the model image of Figure 3(c) with spatial resolutions of 1 nm (a), 0.7 nm (b), and 0.45 nm (c). Corresponding profiles of strain along the growth direction are shown in (d), (e), and (f), respectively. Note that undulations in strain profiles are due to the filtering in the reciprocal space.

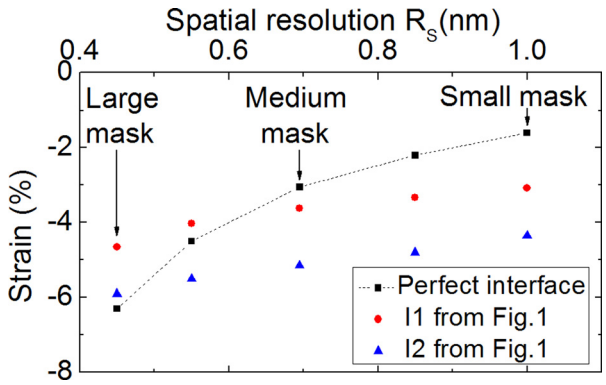

FIG. 6. Evolution of the maxima of strains ($\varepsilon_{\perp}^{GPA}$) measured at interfaces in simulated image (Figure 4(c)) and for the I1 and I2 interfaces in the experimental image (Figure 1(a)) as a function of the spatial resolution R_S.

To conclude, high quality atomically resolved images obtained by HAADF-STEM were studied by combining strain and intensity analyses. All these different approaches converge to demonstrate a high content of AlAs bonds at interfaces spontaneously assembled in InAs/AlSb multilayers for QCLs. The actual interfaces are not perfect but extend over 2 or 3 monolayers. With the best spatial resolution allowed by the mask used in GPA, negative strain of about -6% was measured at interfaces which is of the same order of magnitude as measured in an image generated from a model structure with perfect AlAs interfaces. Nevertheless, the exact value of strain cannot be accurately given due to abrupt strain variations. These results are not restricted to this system but could be applied to other systems that present abrupt interfaces associated with lattice parameter variation.

The authors want to thank Catherine Crestou for the sample preparation. This work is supported by the French research national agency project NAIADE (No. ANR-11-BS10-017). The research leading to these results has received funding from the European Union Seventh Framework Programme under Grant Agreement No. 312483–ESTEEM2 (Integrated Infrastructure Initiative–I3).

[1]K. Mahalingam, H. J. Haugan, G. J. Brown, and K. G. Eyink, Ultramicroscopy **127**, 70 (2013).
[2]J. Nicolaï, B. Warot-Fonrose, C. Gatel, R. Teissier, A. N. Baranov, C. Magen, and A. Ponchet, J. Appl. Phys. **118**, 035305 (2015).
[3]J. Nicolai, Ch. Gatel, B. Warot-Fonrose, R. Teissier, A. N. Baranov, C. Magen, and A. Ponchet, Appl. Phys. Lett. **104**, 031907 (2014).
[4]B. Bonef, L. Gérard, J. L. Rouvière, A. Grenier, P. H. Jouneau, E. Bellet-Amalric, H. Mariette, R. André, and C. Bougerol, Appl. Phys. Lett. **106**, 051904 (2015).
[5]B. Bonef, B. Haas, J. L. Rouvière, R. André, C. Bougerol, A. Grenier, P. H. Jouneau, and J. M. Zuo, J. Microsc. **262**, 178 (2016).
[6]G. Tuttle, H. Kroemer, and J. H. English, J. Appl. Phys. **67**, 3032 (1990).
[7]J. Spitzer, A. Hopner, M. Kuball, M. Cardona, B. Jenichen, H. Neuroth, B. Brarand, and H. Kroemer, J. Appl. Phys. **77**(2), 811 (1995).
[8]O. Cathabard, R. Teissier, J. Devenson, J. C. Moreno, and A. N. Baranov, Appl. Phys. Lett. **96**, 141110 (2010).
[9]V. Swaminathan and A. T. Macrander, *Materials Aspects of GaAs and InP Based Structures* (Prentice-Hall, Inc., Englewood Cliffs, New Jersey, 1991).
[10]M. J. Hÿtch, E. Snoeck, and R. Kilaas, Ultramicroscopy **74**, 131 (1998).
[11]S. J. Pennycook, Ultramicroscopy **30**, 58 (1989).
[12]E. J. Kirkland, R. F. Loane, and J. Silcox, Ultramicroscopy **23**, 77 (1987).
[13]J. P. Peters, R. Beanland, M. Alexe, J. W. Cockburn, D. G. Revin, S. Y. Zhang, and A. M. Sanchez, Ultramicroscopy **157**, 91 (2015).
[14]P. A. Stadelmann, Ultramicroscopy **21**, 131 (1987).